2022-07-15

Distribution and transport of microplastics in groundwater (Shiraz aquifer, southwest Iran)

Esfandiari, A

http://hdl.handle.net/10026.1/19528

10.1016/j.watres.2022.118622
Water Research
Elsevier

Distribution and transport of microplastics in groundwater (Shiraz aquifer, southwest Iran)

Atefeh Esfandiari [a], Sajjad Abbasi * [b,c], Ahmad Behruj Peely [b], Dariush Mowla [a], Mohammad Ali Ghanbarian [b], Patryk Oleszczuk [c], Andrew Turner [d]

[a] Environmental Research Centre in Petroleum and Petrochemical Industries, Department of Chemical Engineering, School of Chemical and Petroleum Engineering, Shiraz University, Shiraz, Iran

[b] Department of Earth Sciences, College of Science, Shiraz University, Shiraz 71454, Iran

[c] Department of Radiochemistry and Environmental Chemistry, Faculty of Chemistry, Maria Curie-Skłodowska University, Lublin 20-031, Poland

[d] School of Geography, Earth and Environmental Sciences, University of Plymouth, Plymouth PL4 8AA, UK

* Corresponding author. Department of Earth Sciences, College of Science, Shiraz University, 71454, Shiraz, Iran; Department of Radiochemistry and Environmental Chemistry, Faculty of Chemistry, Maria Curie-Skłodowska University, Lublin 20-031, Poland. E-mail address: sajjad.abbasi.h@gmail.com; sajjad.abbasi@shirazu.ac.ir

Accepted 13 May 2022

https://doi.org/10.1016/j.watres.2022.118622

Abstract

Despite the significance of groundwater to the hydrological cycle and as a source of potable water, very little information exists on microplastics (MPs) in this environment. In the present study, MPs have been determined in ten well samples obtained from an alluvial aquifer in a semi-arid region (Shiraz, Iran) following filtration, digestion and inspection under a binocular microscope. A total of 96 MPs were identified, and concentrations ranged from 0.1 to 1.3 MP L^{-1} (mean and median = 0.48 and 0.43 MP L^{-1}, respectively) and exhibited a complex distribution across the area that reflected differences in land use and local hydrology and geology. The majority of MPs (about 70%) were fibres of $\leq$ 500 μm in length, but fragments and films were present at some sites, and the dominant polymers were polystyrene, polyethylene and polyethylene terephthalate. Coupling meteorological and water table monitoring data from the regional water organization and published information on aquifer hydrology, we estimate a lag time from precipitation to water table intrusion of between one and five months and groundwater velocity flows of between 0.01 and 0.07 m d^{-1}. Although the extent of retardation of MPs within the pores of groundwater is unknown, by considering empirical data and theoretical predictions on particle flow through porous media in the literature we surmise that MP residence times in the aquifer are likely to range from months to decades, thereby impeding any clear means of source identification. Nevertheless, and more generally, the consumption of potable groundwater may make to a contribution to MP exposure through ingestion.

Keywords: groundwater; fibres; precipitation; transport; hydrogeology; modelling

1. Introduction

Groundwater plays a critical role in the hydrological cycle and, in the form of aquifers, is an important water resource. In arid and semi-arid regions, aquifers are particularly valuable for socio-economic development, acting as a source of water for drinking, agriculture and industry (Scanlon et al., 2006; Hssaisoune et al., 2020). However, because of the demands on aquifers in populated areas, abstraction may well exceed recharge and depletion of groundwater takes place. In addition to resource loss, diminishing reserves may be associated with drying of springs, abandonment of wells, increased pumping costs and, depending on local geology, a reduction in water quality (Rodríguez-Estrella, 2012).

Inadequate water and waste management and treatment and poor agricultural and industrial practices can also lead to the contamination of groundwater by a variety of substances, with consequences for human health and the local environment and ecosystems. Specifically, excessive applications of agrochemicals can result in high groundwater levels of nitrate, pesticides and potassium (Oren et al., 2004; Abdesselam et al., 2013; El Alfy and Faraj, 2016), while urban runoff and waste water and the use of untreated water for irrigation may adversely impact on levels of chemical oxygen and may introduce road salts, oils, metals, pharmaceuticals and pathogens (Fernández-Cirelli et al., 2009, Abd-Elaty et al., 2021; Li et al., 2021).

Another type of contaminant that is both persistent and pervasive is microplastics (MPs), or plastics whose primary diameters are less than 5 mm. The distribution, behaviour, impacts and fate of MPs have been extensively studied in the marine and fresh water environments, and in soils and the atmosphere (da Costa et al., 2018; Ng et al., 2018; Allen et al., 2019; Abbasi and Turner, 2021; Coyle et al., 2021; Tanentzap et al., 2021), but there is very little study of MPs in the subsurface environment. Minteneg et al. (2018) provided evidence for the presence of MPs in groundwater by detecting small quantities (< 7 MP m^{-3}) in groundwater sampled from wells at more than 30 m depth in north west Germany. Panno et al. (2018) found significantly higher concentrations of MPs (up to 15.2 MP L^{-1}) that were all fibrous in nature in springs and wells from two more open karst aquifers in Illinois, USA, and attributed their presence, largely, to septic effluent. Most recently, Samandra et al. (2022) found concentrations of MPs that were mainly fragments and fibres averaging about 40 MP L^{-1} in groundwater sampled from capped monitoring bores in an alluvial aquifer in Victoria, Australia. Because of the abundance of alluvial aquifers globally, the authors called for further research into this type of system.

We present the first study of MPs in an alluvial aquifer from a semi-arid region (Shiraz, southwest Iran). High volume samples are taken from a number of observation (monitoring) wells and MPs are isolated, identified and characterized according to established techniques. We also utilize seasonal distributions of rainfall and water table depth for the region to provide a semi-quantitative assessment of the velocities of MPs in groundwater and the timescales that they may reside in the subsurface environment.

2. Methods

2.1. Study area and hydrogeological characteristics

The geology and hydrology of the Shiraz watershed and aquifer are shown in Figures 1a and 1b, respectively. Shiraz watershed is located within the Zagros foreland folded belt of the Fars province of southwest Iran and is about 1450 km^2 in area (Jafari et al. 2021), with the highest elevations in the northern reaches (The Ghalat Mountains; about 2900 m) and the lowest elevations towards Maharloo Lake in the south (about 1430 m). Annual average precipitation at Galat and Shiraz meteorological stations is 480 and 354 mm, respectively, with most precipitation falling between the months of November and March. The principal rivers (the Khoshk and its tributary, the Azam) drain the catchment on a seasonal basis and head in a southeasterly direction, passing through Shiraz city and recharging the lake. According to Jafari et al. (2021), land use is dominated by pasture and bare land, with smaller contributions from urban, agriculture, orchard, forest and wetland, and soils are heterogeneous and erosive silty and sandy loams.

Shiraz aquifer occupies an area of about 300 km^2 in the Shiraz watershed and is an unconfined alluvial system surrounded by karstic limestone (and mainly Asmari-Jahrum) formations. Quaternary deposits consist of coarse-grained sediments and medium- to fine-grained clastic materials, but closer to Maharloo Lake sediments become finer and admixed with halite and gypsum (Tajabadi et al., 2018). The aquifer has an average thickness of 30 m where unconfined, and mean water table depth generally ranges from about 35 m to the north and west to < 3 m in the south (where greater evaporation and mixing with lake water results in more saline water; Tajabadi et al., 2018; Jafari et al., 2021). However, because of vertical granulometric variations, confined groundwater can be found at depths exceeding 200 m in some places (Baghapour et al., 2016). The general flow is from the northwest to the southeast, and interactions with the Khoshk River are restricted to the southeast of the aquifer. Land use within the region is mainly residential, cultivated and, towards the lake, barren because of soil salinization (Amiri et al., 2015). Although the region relies heavily on groundwater resources for economic and demographic development, contamination from wastes, and in particular by nitrate from agriculture, present a pervasive problem (Baghapour et al., 2016; Alamdar et al., 2019).

The approximate boundary of the aquifer and contours of water table elevation are shown in Figure 1b. Water table levels and depths obtained from the Shiraz Regional Water Organization were interpolated using inverse distance weighting (Charizopoulos et al., 2018), with water table elevation contours subsequently extracted from the water table raster file using ArcMap 10.8. Note the decline in water table elevation from over 1700 m in the north to < 1460 m in the south; note also that the southern and eastern boundaries could not be as accurately defined from available data.

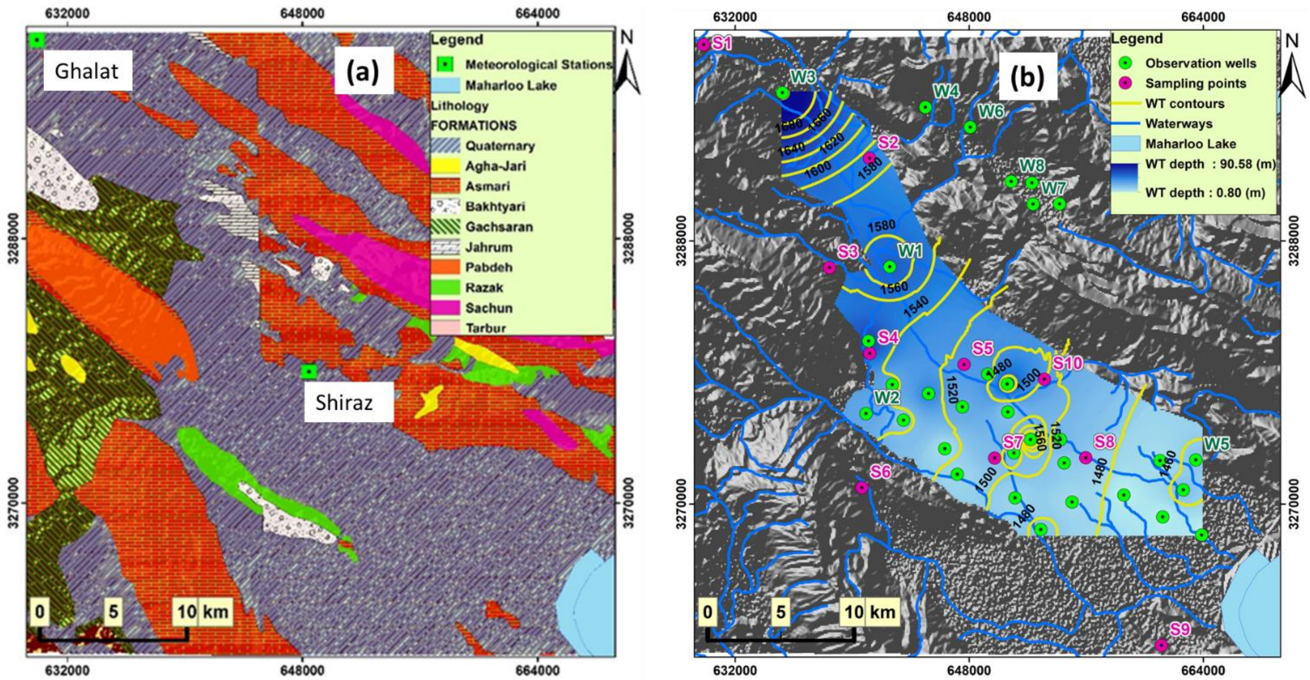

Figure 1: (a) The geology of the Shiraz watershed, from the Galat Mountains (northwest) to Maharloo Lake (southeast), illustrating the distribution of Quaternary deposits and surrounding karstic limestones. (b) The approximate, modelled boundary of Shiraz alluvial aquifer, mean contours of water table elevation (in m above sea level and at 20 m intervals) and seasonal, surface waterways. Wells used to map the aquifer are show in green (n = 32), with the eight used for time lag modelling numbered, and wells shown in pink (n = 8) are where MPs were sampled from.

2.2. Sample collection

Groundwater samples were obtained from ten wells located throughout Shiraz aquifer (and just beyond its modelled boundary but within Quaternary deposits) in May 2021 (Figure 1b and Table 1). Wells in the region are open, with flow rates ranging from < 3 to about 90 L s^{-1}. Most are lined with 10 to 50 cm-diameter stainless steel, but some are lined with black polyethylene. In the unsaturated zone, liners are supported by and sealed with cement grout, while below this zone, liners are perforated and encased in stainless steel mesh whose pore size is variable (but generally around 1-2 mm) or unknown. At each site, the pump was turned on and water was allowed to flow for about fifteen to thirty minutes in order to minimize contamination from direct atmospheric deposition into the well. Samples of 20 L were then collected in two custom-made ~ 10-L amber glass bottles that had been pre-rinsed with filtered (< 2 μm) water by an operator wearing latex gloves and cotton clothing.

Table 1: Coordinates and elevation of the wells sampled and estimates of mean water table (WT) depth based on interpolation of the contours shown in Figure 1b.

Location	X	Y	elevation, m	WT depth, m
S1	629860	3301408	1984	184
S2	641200	3293634	1740	150
S3	638448	3286167	1771	201
S4	641206	3280305	1594	44
S5	647648	3279552	1569	69
S6	640674	3271120	1561	31
S7	649741	3273149	1516	1
S8	655980	3273165	1492	7
S9	661139	3260341	1471	21
S10	653143	3278537	1585	85

2.3. Microplastic extraction and identification

Well waters were processed in a clean facility and using pre-filtered water and reagents and pre-cleaned consumables and glassware as in our previous studies (Abbasi and Turner, 2021). Briefly, 250 mL of 30% H_2O_2 (Arman Sina, Tehran) was added to each bottle and the contents were left at room temperature for 7 d. Digests from each location (i.e. two bottles) were then vacuum-filtered through 150 mm diameter S&S filters (Blue Band, grade 589/3, 2 μm pore size) using a glassporcelain Buchner system, and filters were subsequently dried under aluminium foil in a clean cabinet at room temperature for 24 to 48 h.

Material on each filter was carefully transferred into a series of glass petri dishes using a fine, horsehair brush and MPs were identified using a binocular microscope (Carl-Zeiss) at up to 200 x magnification with the aid of a 250 μm-diameter stainless steel probe and ImageJ software. Identification was based on shininess, cross-sectional properties, surface structure, thickness, hardness and reaction to the heated probe and according to criteria given by Hidalgo-Ruz et al. (2012) and De Witte et al. (2014). Particle size was classified in terms of the longest dimension or, for fibres, length, L, as $\leq$ 100 μm, 100 < $L \leq$ 250 μm, 250 $\leq L$ < 500 μm, 500 $\leq L$ < 1000 μm or $\geq$ 1000 μm, colour was classified as white-transparent, blue-green, red-yellow or black-grey, and shape was classified as fibre (with a length to diameter ratio exceeding three), film, fragment or spherule-granule.

Negative controls, derived by processing 2 x 20 L of filtered water as above and microscopically inspecting the resulting residues revealed no MP contamination arising from the containers or laboratory. Positive controls consisted of ten polyethylene fragments and ten polyvinyl chloride fragments (both white and 20 to 250 μm in diameter sourced from Eppendorf) added, with the aid of tweezers and the microscope, to separate 20-L volumes of filtered water. Processing these controls likewise full recovery in both cases.

The most commonly encountered MP types and at least one from each well (n = 19 in total) that had been isolated from the groundwater samples were prepared for further characterization. Samples were firstly mounted on conductive copper adhesive tape and analysed for polymeric composition using a micro-Raman spectrometer (LabRAM HR, Horiba, Japan) configured with a laser at 785 nm, a Raman shift of 400-1800 cm^{-1} and acquisition times of 20 to 30 seconds. A high vacuum scanning electron microscope (SEM; TESCAN Vega 3, Czech Republic) with a resolution of 2 nm and an accelerating voltage of 20 kV was then used to assess the surface morphology of a further selection of MPs (n = 11) that had been placed on microscope slides and gold-coated.

2.3. Modelling rainfall-groundwater lag time

In order to estimate how long it takes rain water and, therefore, any soluble contaminant washed out from the atmosphere, to reach groundwater, correlograms were generated for eight of the observation wells shown in Figure 1b according to methods outlined in Samani (2001) and using data supplied by the Shiraz Regional Water Organization.

A correlogram is a plot of the cross-correlation coefficient, $r_{xy}(k)$, as a function of lag, k, and is defined as follows:

$$r_{xy}(k) = \frac{C_{xy}(k)}{\sqrt{C_{xx}(0)C_{yy}(0)}} \qquad (1)$$

where $C_{xy}(k)$ is the coefficient of cross covariance at lag k for time series $x(t)$ and $y(t)$:

$$C_{xy}(k) = \frac{1}{n-k}\sum_{i=1}^{n-k} x_i y_{i+k} - \frac{1}{n^2}\sum_{i=1}^{n} x_i \sum_{i=1}^{n} y_i \qquad (2)$$

and $C_{xx}(0)$ and $C_{yy}(0)$ are the variances at lag zero for x and y, respectively:

$$C_{xx}(0) = \frac{1}{n}\sum_{i=1}^{n}(x_i - \bar{x})^2 \qquad (3)$$

$$C_{yy}(0) = \frac{1}{n}\sum_{i=1}^{n}(y_i - \bar{y})^2 \quad (4)$$

In the time series of some wells, it was difficult to detect a meaningful relationship between the rainfall and water level because of autocorrelation and data processing was necessary to eliminate or reduce noise. In this context, firstly decomposition of trend and seasonality was applied. Secondly, autoregressive integrated moving average (ARIMA), which is a statistical analysis model using a combination of the differenced autoregressive model with the moving average model, was applied to the residuals arising from the first step to better understand the data set. These steps were continued on the two time series until no trends, patterns or autocorrelation were observed and the cross correlation was applied to the residuals from the ARIMA analysis.

All calculations and correlations were performed in Minitab® 16.2.0 and correlograms were generated in Excel 2013. The maximum value of $r_{xy}(k)$ observed in a periodic component of the correlogram was defined as the lag time between rainfall and groundwater level response.

3. Results

3.1. Quantities and characteristics of microplastics

A selection of MPs identified under the microscope is shown in Figure 2 and the number and nature of MPs detected in the groundwater samples are presented in Table 2. Thus, overall 96 MPs were observed with numbers in individual 20-L samples ranging from 2 (S4) to 26 (S8) (mean =

9.8, median = 8.5). The lowest quantities of MP were found in regions relatively remote from urbanization (the Ghalat Mountains in the northwest of the region and towards Maharloo Lake in the southeast). However, the greatest concentrations were not encountered in the vicinity of Shiraz City but were located to the west of the region.

Fibres were the dominant MP shape (about 70%), with fragments and films contributing about 20% and 10%, respectively. All MPs detected were $\leq$ 500 μm in size, with abundance increasing with decreasing size range and about 60% of MPs encountered below 100 μm. Although MPs were encountered in all colour categories, black-grey and red-yellow were most common overall and white-transparent and blue-green were most common for non-fibrous particles.

Table 2: Numbers, categories (by shape) and characteristics (colour and size, where L = longest dimension or length) of the MPs retrieved from the ten groundwater samples whose locations are shown in Figure 1.

location or category	fibres	films	fragments	total
S1	1		2	3
S2	6	1	5	12
S3	6	1		7
S4	21	3	2	26
S5	7		3	10
S6	12		1	13
S7	3		2	5
S8	2			2
S9	5	4	4	13
S10	5			5
total	**68**	**9**	**19**	**96**
$L \leq 100$ μm	41	3	12	56
$100 < L \leq 250$ μm	20	3	7	30
$250 < L \leq 500$ μm	9		1	10
white-transparent	4	3	6	13
blue-green	12	3	5	20
red-yellow	22	2	5	29
black-grey	30	1	3	34

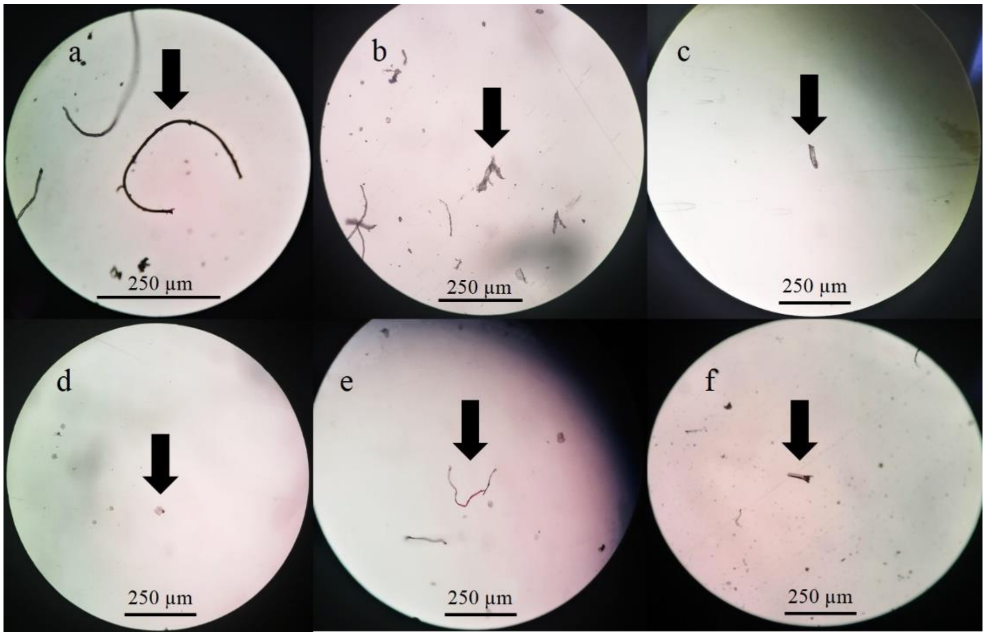

Figure 2: Examples of MP fibres (a and e), fragments (b and f) and films (c and d) retrieved from the groundwater samples and identified under the microscope. Note that much of the remaining material shown, including several additional fibres, was non-plastic.

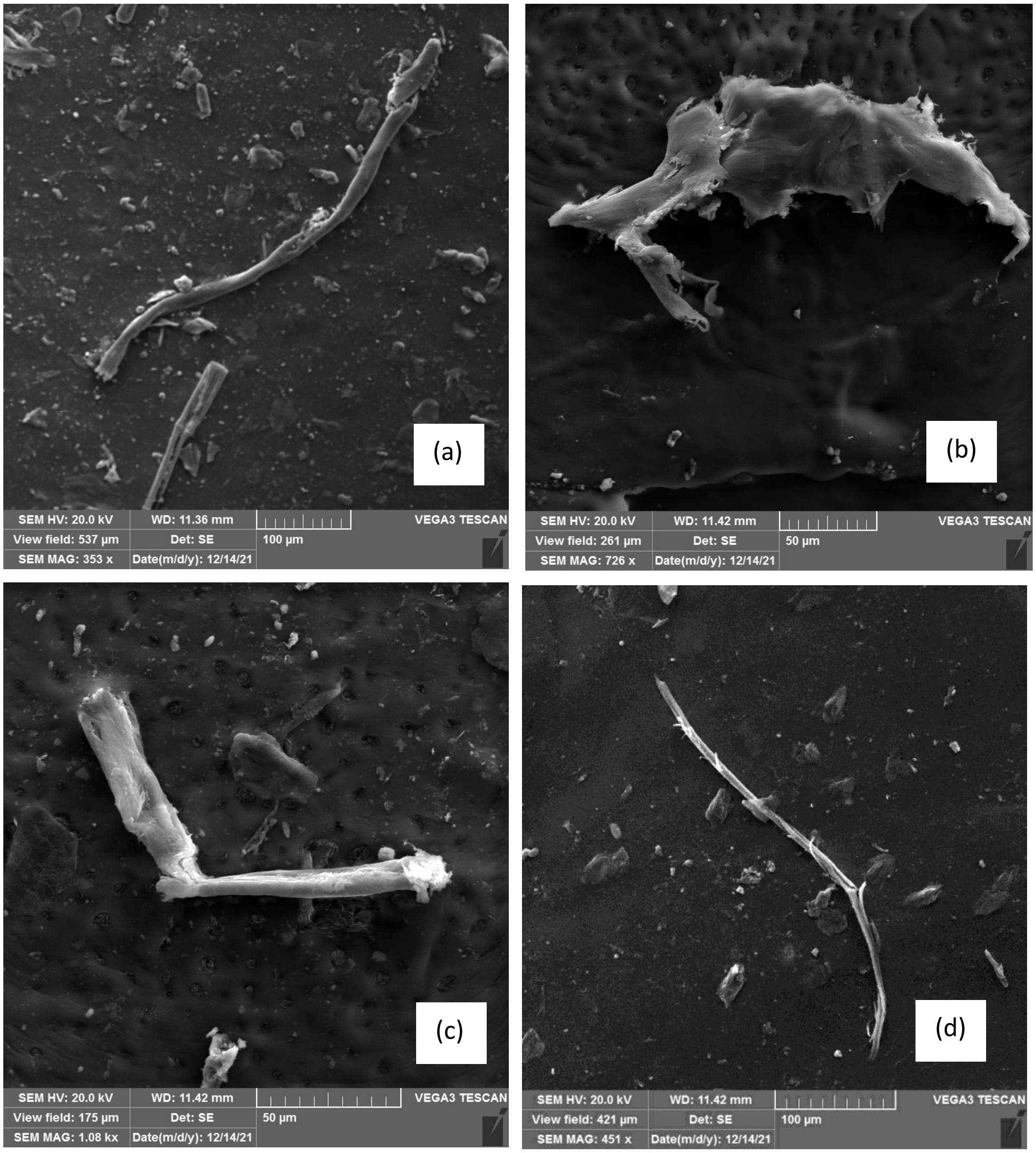

Figure 3: SEM images of three MP fibres (a, c and d) and a film (b) sampled from the groundwater wells.

The surfaces of MPs captured by SEM are exemplified in Figure 3. There is evidence of oxidation on the surfaces of some samples (e.g., flaking and pits in Figures 3b and 3c) whereas the surfaces of other MPs appear to be relatively smooth (e.g. Figures 3a and 3d). Physical damage is evident in all cases that includes fracturing, twisting, cleavage and deformation.

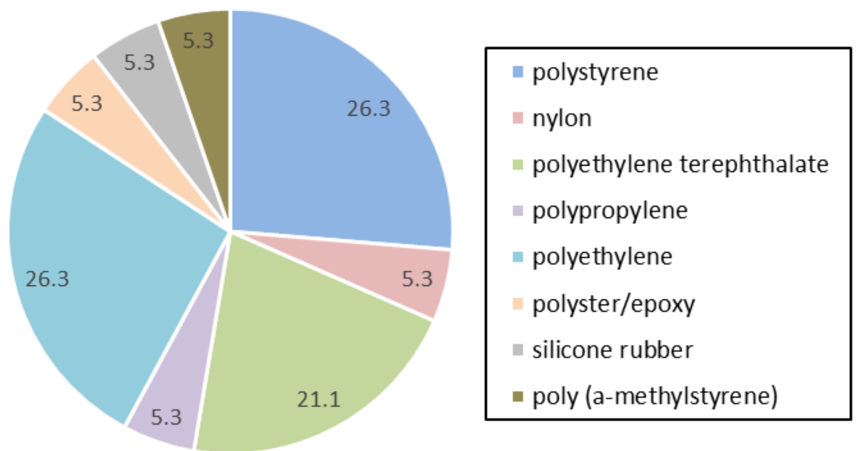

Figure 4: Percentage distribution of selected MPs (n = 19) by polymer type.

The distribution of selected MPs (~20% in total, and including fibres, fragments and films) is shown by polymer type in Figure 4. More than one-half of MPs were constructed of polystyrene or polyethylene, with an additional sample based on the styrenic compound, poly (α-methylstyrene). Four samples were constructed of polyethylene terephthalate, with four additional polymers or polymer combinations (including a rubber) encountered amongst the remaining samples. These polymers encompass a range of densities from below 1 g cm^{-3} (polyethylene, polypropylene, poly (α-methylstyrene)) to about 1.4 g cm^{-3} (polyester and polyethylene terephthalate). Significantly, only one sample had the same colour and construction as the lining material used in some of the wells (black polyethylene) suggesting that a small degree of contamination from the well structure itself is possible.

3.2. Meteorological and hydrological data

Monthly rainfall and water table levels, based on available data between 2001 and 2018-2019 held by the Shiraz Regional Water Organization, are plotted as a function of time in Figure 5. Here, water table elevations for six wells to the north of the region are plotted with rainfall data for Ghalat and water table elevations for six wells in the central and southern regions are plotted with rainfall data for Shiraz. At both stations and over the period considered, the seasonality in rainfall is clear and a net reduction in annual rainfall is evident. There is also evidence of an increase in the depth of the water table in many of the time series but rainfall-driven seasonality to this depth is also evident in most cases.

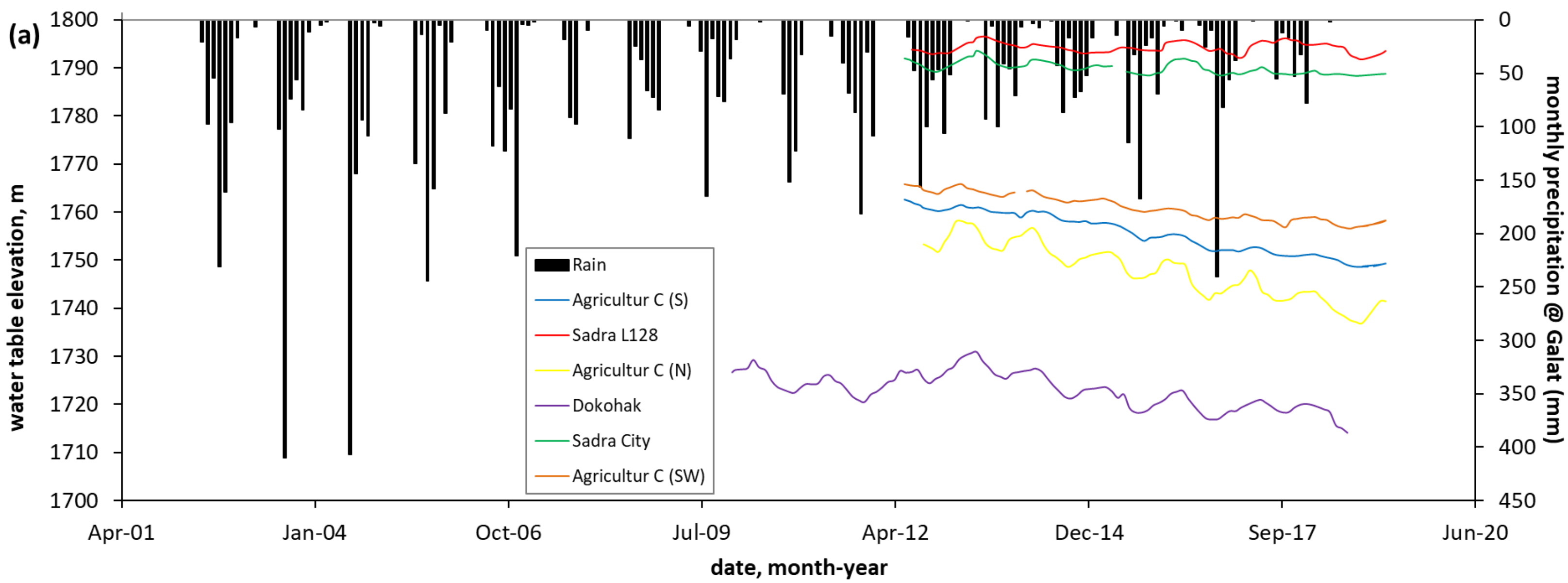
(a)
water table elevation, m
monthly precipitation @ Galat (mm)
date, month-year
Rain
Agricultur C (S)
Sadra L128
Agricultur C (N)
Dokohak
Sadra City
Agricultur C (SW)

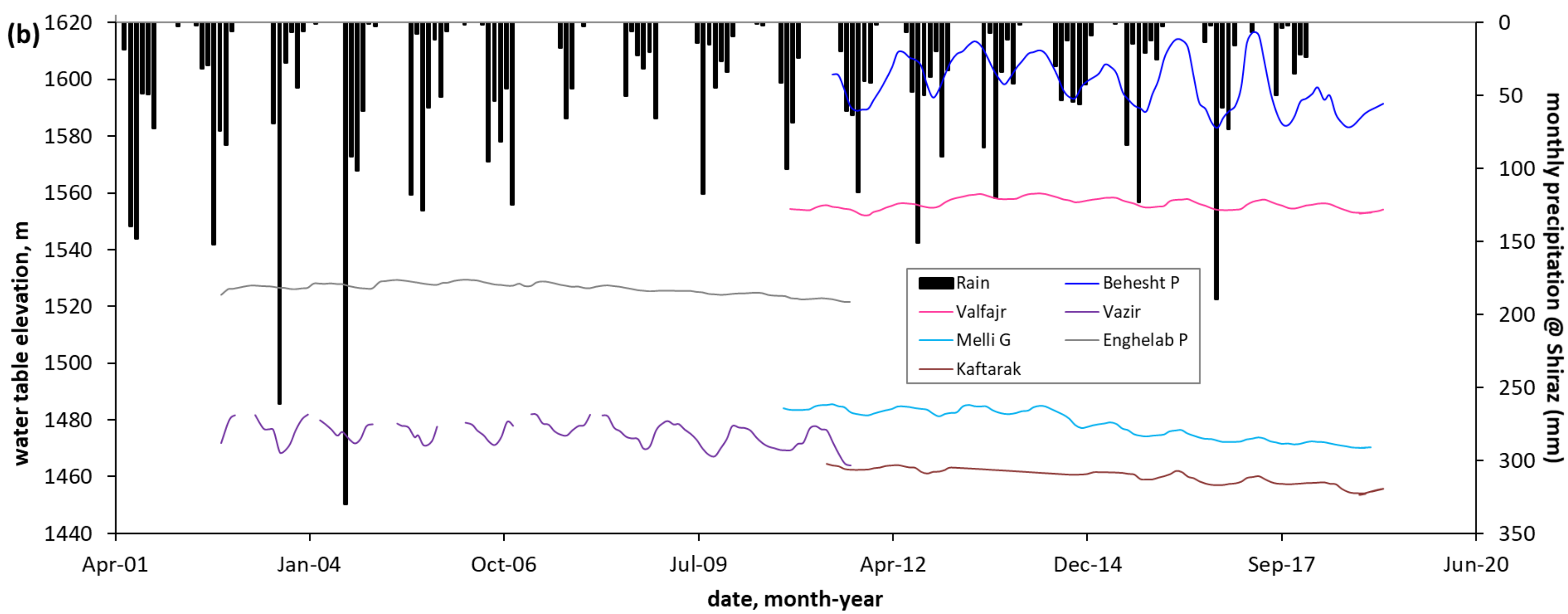
(b)
water table elevation, m
monthly precipitation @ Shiraz (mm)
date, month-year
Rain
Valfajr
Melli G
Kaftarak
Behesht P
Vazir
Enghelab P

Figure 5: Temporal distribution of monthly rainfall and water table level for twelve named observation wells (six using Ghalat precipitation data and six using Shiraz precipitation data).

3.3. Cross correlograms and lag time estimation

The cross-correlograms arising from the rainfall and water table data for eight observation wells is shown in Figure 6. Oscillations with negligible damping indicate the presence of a periodic component in the total data set and the value of k where $r_{xy}(k)$ is a maximum (the central peak for each correlogram) provides an estimate of the time lag between rainfall and its intrusion into groundwater (Samani et al., 2001). Values of k are shown for each well considered in Table 3 and indicate lags of between one and five months. Note, however, that the three estimates for one month are associated with the greatest uncertainties (lowest cross-correlation coefficients and least distinctive central peaks). Overall, there is no clear spatial pattern or statistical relationship with water table depth, with the greatest time lags (towards the north of the region) associated with the highest elevations but not the lowest water table depths. Presumably, distributions are dependent on additional factors such as the precise granulometry of Quaternary deposits, proximity to specific geological features and the abundance and nature of any impervious surfaces and drainage systems.

Table 3: Coordinates, elevations and mean water table (WT) depths for the wells used to generate the correlograms, and cross-correlation coefficients ($r_{xy}(k)$) and estimates of lag time (k) derived from the plots in Figure 6.

Location	X	Y	elevation, m	WT depth, m	rainfall data	$r_{xy}(k)$	k, months
Behesht P	642582	3286229	1649	54	Shiraz	0.575	2
Valfajr	640950	3276187	1583	28	Shiraz	0.380	3
Dokohak	635239	3298122	1811	91	Galat	0.382	2
Sadra City	645008	3297135	1813	23	Galat	0.417	4
Kaftarak	663501	3273019	1470	16	Shiraz	0.274	1
Sadra L128	648077	3295764	1819	24	Galat	0.390	5
Agricultur C (S)	652372	3290516	1787	39	Galat	0.278	1
Agricultur C (SW)	650875	3292055	1786	30	Galat	0.151	1

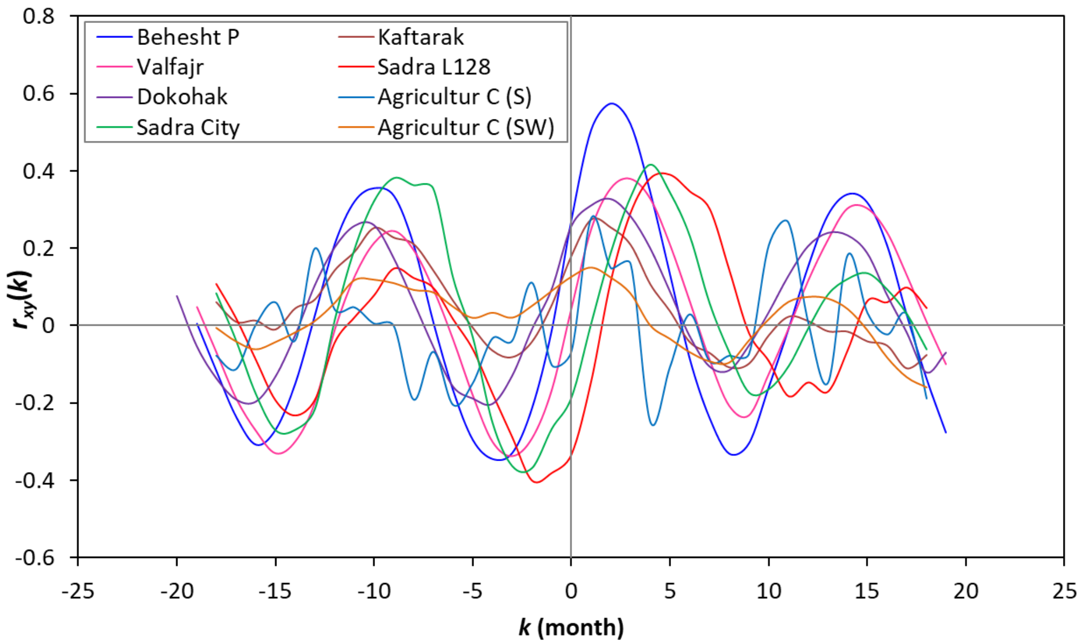

Figure 6: Cross-correlograms (cross-correlation coefficient, $r_{xy}(k)$, as a function of lag, k) for rainfall and water table level at eight observation wells.

4. Discussion

The concentrations of MPs detected on a number basis in groundwater of Shiraz range from 0.1 to 1.3 MP L^{-1} (mean and median = 0.48 and 0.43 MP L^{-1}, respectively). These are lower than concentrations reported for wells and springs sampled from a more open and creviced karst aquifer in Illinois (up to 15 MP L^{-1}; Panno et al., 2019) and are considerably lower than concentrations of recently reported for unconfined alluvial aquifers in Victoria, Australia (16 to 97 MP L^{-1}; O'Connor et al., 2019). Concentrations in the present study are, however, higher than those reported for groundwater from five of regions of Germany (up to 0.007 MP L^{-1}; Mintenig et al. 2019) and abstracted from chalk and sandstone aquifers in the UK after treatment by disinfection or filtration (up to 0.0107 MP L^{-1}; Johnson et al., 2020). Presumably, these differences reflect variations in hydrogeology, land use, MP sources, means of MP sampling and identification (including size detection limits), and the presence or nature of any water treatment. We also note that, consistent with our observations, Johnson et al. (2020) report polystyrene as the most abundant polymer type, despite the relatively small demand for this plastic compared with polyolefins (Andrady and Neal, 2009).

A more useful, quantitative comparison of MPs in Shiraz groundwater is with MPs in precipitation from the same region that have been collected and processed by similar protocols. Thus, according to Abbasi and Turner (2021), concentrations of MPs in monthly precipitation identified microscopically after sample peroxidation are 150 to 2220 MP L^{-1} (mean = 280 MP L^{-1}; median = 75 MP L^{-1}) in Shiraz City and 30 to 680 MP L^{-1} (mean = 84 MP L^{-1}; median = 15 MP L^{-1}) in the mountains to the northwest. Despite concentrations in Shiraz groundwater being two or three orders of magnitude lower than concentrations in local precipitation, the particle size distributions are similar with the largest contributions to each sample type arising from the $\leq$ 100 μm fraction.

Once precipitation encounters the ground it will interact with additional MPs deposited during dry episodes; in the present setting, extended (seasonal) periods of dry weather may allow considerable accumulation of MPs on porous and rough surfaces, with initial rainfall acting to "flush" MPs through water film expansion-release (O'Connor et al., 2019). In agricultural soils, additional MPs may also be introduced through the application of plastic-based mulches (Huang et al., 2020), biosolids used as fertilizers (Crossman et al., 2020) and contaminated irrigation waters (Liu et al., 2018; Kumar et al., 2020), with measurements in the region of Shiraz revealing an average of about 0.5 MP per g of surface and subsurface soil (Rezaei et al., 2022). A proportion of precipitation, coupled with any irrigation water, will infiltrate permeable surfaces with its loading of MPs. This load will be modified by the capture or adhesion and retention of MPs in the substrate and, possibly, the remobilization of previously captured particles by the lower ionic strength of percolating rainwater (Goeppert and Goldscheider, 2021). A reduction in MP concentration from precipitation to groundwater observed in the present study suggests significant net removal during infiltration.

Variations in MP concentrations observed in groundwater throughout the region reflect variations in dry and wet deposition rates, land use (including application of irrigation water), surface permeability and infiltration rates, underlying geology and granulometry, and depth of the water table. For instance, one of the lowest MP concentrations was encountered in the remote and most elevated region of the Ghalat Mountains (S1) where plastic deposition is, presumably, minimal, and the mean water table is located at about 180 m below the surface; under these conditions, the concentration of MPs serve as a regional baseline. The highest concentrations of MPs were encountered to the west of Shiraz City (S4 and S6) where MP inputs are augmented by agricultural activities (including use of urban waste waters for irrigation; Rezaei et al., 2022), infiltration is promoted by extensive ploughing, and the vertical transport of groundwater is expedited by the Sabz Pushan fault (Lacombe et al., 2006). Samples from the most populated and industrialized districts of Shiraz City itself (S5 and S10) exhibit moderate concentrations of MPs, despite a multitude of sources of MPs in the urban setting (Abbasi et al., 2017; Grbic et al., 2020). This may be attributed to the abundance of impermeable surfaces (roads and buildings) that limit exchange with the subsurface environment.

The MPs retrieved from the wells of the Shiraz aquifer are irregular in shape (and mainly fibrous) and degree of weathering, and are heterogeneous in polymer makeup and density (including both positively and negatively buoyant particles). It is surmised that those sampled reflect a combination of MPs that have migrated vertically from the surface to the water table, and taking at least one to five months to do so depending on the geological, hydrological and land-use factors described above, and those that have, additionally, been transported along the gradient of the water table. Based on a median hydraulic conductivity for Shiraz aquifer of 12 m d^{-1} (Baghapour et al., 2016), a hydraulic gradient ranging from 0.006 in the alluvial fans to 0.001 in the vicinity of the Maharloo Lake (Tajabadi et al., 2018) and a transmissivity of 86.4 m^2 d^{-1} (Masoomi, 2016), groundwater flows and flow velocities are estimated to be between 0.09 and 0.6 m^3 d^{-1} and about 0.01 and 0.07 m d^{-1}, respectively.

While the hydraulic timescales referred to above define the periods involved in the vertical and lateral diffusive transportation of soluble contaminants, it would be expected that MPs are impeded through physical, hydrophobic and, if sufficiently oxidized, chemical and electrostatic interactions with the substrate. O'Connor et al. (2019) studied the vertical migration of polyolefin-based plastics of diameter 21-535 μm in sand-soil columns subject to different environmental conditions. Migration was greatest for the finest MPs but was predicted to be limited to a few m over many years. In contrast, at a large-scale alluvial aquifer test site, Goeppert and Goldscheider (2021) found that polystyrene spheres below 5 μm in diameter travelled up to 200 m along a natural gradient and at velocities up to 6.25 m h^{-1} and, in many cases, more quickly than the diffusion of a tracer solute. These, field-based observations suggest that retardation and filtration are not necessarily important for very fine, regularly-shaped MPs.

There are no direct data available on the movement of more irregularly-shaped MPs, like fibres, in soils. However, a general theoretical framework that is applicable to large fibre-like colloids was presented by Engdahl (2018). Here, the physical filtration of massless, non-interacting fibres of constant length (and treated as bead-rod chains) was simulated through a poorly consolidated, coarse-grained alluvial deposit (mean pore water velocity = 26 m d^{-1}) using a "random obstacle model". The shortest fibres considered (~ 1.3 mm) were smaller than the average pore size of the medium and could be transported unimpeded as they readily aligned with the velocity field. These fibres could also progress more quickly than a passive tracer because of their ability to bypass slow moving regions. Longer fibres (up to 3.3 mm) were subject to bending, flipping and rolling and were more readily retarded by wrapping around grains. Simulations performed at lower speeds exhibited less retardation than faster simulations and in each case the magnitude of the filtration speed was proportional to the length of the fibre.

Based on experimental observations and theoretical simulations, and neglecting any interactions arising from friction, flocculation and electrostatics, the slow velocity fields of the Shiraz aquifer are predicted to favour the transport of regularly-shaped MPs and fibres that are smaller (or shorter) than the mean pore size of the medium, including those evading detection in our analysis, with larger MPs impeded by physical constraints. Regardless of the degree of retardation, however, the flow velocities involved across the 50 km northwest-southeast axis of the Shiraz aquifer suggest that MPs may reside in the system for years to decades, hampering any clear means of source identification.

5. Conclusion

The present study is the first to document the presence, concentrations and characteristics of MPs in an aquifer from a semi-arid region, and only the second to report MPs in an alluvial groundwater system. MP concentrations are heterogeneous throughout the Shiraz aquifer and range from 0.1 to 1.3 MP L^{-1}, with fibres $\leq$ 500 μm in length the dominant shape and polyethylene, polystyrene and polyethylene terephthalate the most important polymers. MP heterogeneity is attributed to different land-uses, including variable agricultural practices, and variations in local geology, permeability and infiltration rates. Based on time lags between precipitation and intrusion into the aquifer, groundwater flow rates and retardation of fine particulate material in porous media, we predict that MPs are likely to reside in the Shiraz aquifer system for years to decades. Nevertheless, because groundwater is frequently used as a supply of potable water, its consumption may make to a contribution to human exposure through ingestion.

Acknowledgements

We thank Shiraz University for funding the study (grant no. 99GRC1M371631).

References

Abbasi, S., Turner, A., 2021. Dry and wet deposition of microplastics in a semi-arid region (Shiraz, Iran). Science of the Total Environment 786, 147358.

Abbasi, S., Keshavarzi, B., Moore, F., Delshab, H., Soltani, N., Sorooshian, A., 2017. Investigation of microrubbers, microplastics and heavy metals in street dust: a study in Bushehr city, Iran. Environmental Earth Sciences 76, 798.

Abd-Elhamid, H.F., Abd-Elmoneem, S.M., Abdelaal, G.M., Zeleňáková, M., Vranayova, Z., Abd-Elaty, I., 2021. Investigating and managing the impact of using untreated wastewater for irrigation on the groundwater quality in arid and semi-arid regions. Int. J. Environ. Res. Public Health 18, 7485. https://doi.org/10.3390/ijerph18147485

Abdesselam, S., Halitim, A., Jan, A., Troland, F., Bourrié, G., 2013. Anthropogenic contamination of groundwater with nitrate in arid region: case study of southern Hodna (Algeria). Environmental Earth Sciences 70, 2129-2141.

Andrady, A.L., Neal, M.A., 2009. Applications and societal benefits of plastics. Philosophical Transactions of the Royal Society of London B: Biological Sciences 364, 1977-1984.

Allen, S., Allen, D., Phoenix, V.R., Le Roux, G., Jimenez, P.D., Simonneau, A., Binet, S., Galop, D., 2019. Atmospheric transport and deposition of microplastics in a remote mountain catchment. Nature Geoscience 12, 339-344.

Charizopoulos, N., Zagana, E., Psilovikos, A., 2018. Assessment of natural and anthropogenic impacts in groundwater, utilizing multivariate statistical analysis and inverse distance weighted interpolation modeling: the case of a Scopia basin (Central Greece). Environmental Earth Sciences 77, article no. 380.

Coyle, R., Hardiman, G., O'Driscoll, K., 2021. Microplastics in the marine environment: A review of their sources, distribution processes, uptake and exchange in ecosystems. Case Studies in Chemical and Environmental Engineering 2, 100010.

Crossman, J., Hurley, R.R., Futter, M., Nizzetto, L., 2020. Transfer and transport of microplastics from biosolids to agricultural soils and the wider environment. Science of the Total Environment 724, 138334.

da Costa, P.J., Paço, A., Santos, P.S.M., Duarte, A.C., Rocha-Santos, T., 2018. Microplastics in soils: assessment, analytics and risks. Environmental Chemistry 16, 18–30.

De Witte, B.; Devriese, L.; Bekaert, K.; Hoffman, S.; Vandermeersch, G.; Cooreman, K.; Robbens, K., 2014. Quality assessment of the blue mussel (*Mytilus edulis*): Comparison between commercial and wild types. Marine Pollution Bulletin 85, 146-155.

El Alfy, M., Faraj, T., 2016. Spatial distribution and health risk assessment for groundwater contamination from intensive pesticide use in arid areas Environmental Geochemistry and Health 39, 231-253.

Engdahl, N.B., 2018. Simulating the mobility of micro-plastics and other fiber-like objects in saturated porous media using constrained random walks. Advances in Water Resources 121, 277-284.

Fernández-Cirelli, A., Arumí, J.L., Rivera, D., Boochs, P.W., 2009. Environmental effects of irrigation in arid and semi-arid regions. Chilean Journal of Agricultural Research 69, 27-40.

Goeppert, N., Goldscheider, N., 2021. Experimental field evidence for transport of microplastic tracers over large distances in an alluvial aquifer. Journal of Hazardous Materials 408, 124844.

Grbic, J., Helm, P., Athey, S., Rochman, C.M., 2020. Microplastics entering northwestern Lake Ontario are diverse and linked to urban sources. Water Research 174, 115623.

Hidalgo-Ruz, V.; Gutow, L.; Thompson, R.C.; Thiel, M., 2012. Microplastics in the marine environment: A review of the methods used for identification and quantification. Environmental Science & Technology 46, 3060-3075.

Hssaisoune, M., Bouchaou, L., Sifeddine, A., Bouimetarhan, I., Chehbouni, A., 2020. Moroccan groundwater resources and evolution with climate changes. Geosciences 10, 81; doi:10.3390/geosciences10020081

Huang, Y., Liu, Q., Jia, W., Yan, C., Wang, J., 2020. Agricultural plastic mulching as a source of microplastics in the terrestrial environment. Environ. Pollut. 260, 114096. https://doi.org/10.1016/j.envpol.2020.114096.

Johnson, A.C., Ball, H., Cross, R., Horton, A.A., Jürgens, M.D., Read, D.S., Vollertsen, J., Svendsen, C., 2020. Identification and quantification of microplastics in potable water and their sources within water treatment works in England and Wales. Environmental Science and Technology 54, 12326-12334.

Kumar, M., Xiong, X., He, M., Tsang, D.C.W., Gupta, J., Khan, E., Harrad, S., Hou, D., Ok, Y.S., Bolan, N.S., 2020. Microplastics as pollutants in agricultural soils. Environmental Pollution 265, 114980.

Lacombe, O., Mouthereau, F., Kargar, S., Meyer, B., 2006. Late Cenozoic and modern stress fields in the western Fars (Iran): Implications for the tectonic and kinematic evolution of central Zagros. Tectonics 25, TC1003.

Li P., Karunanidhi, D., Subramani, T., Srinivasamoorthy, K., 2021. Sources and consequences of groundwater contamination. Archives of Environmental Contamination and Toxicology 80, 1-10.

Liu, M., Luo, S., Yang, S., Lei, L., Hu, J., Lv, W., Zhou, W., Cao, C., Shi, H., Yang, X., He, D., 2018. Microplastic and mesoplastic pollution in farmland soils in suburbs of Shanghai, China. Environ. Pollut. 242, 855–862.

Masoomi, B., 2016. Estimation of hydraulic parameters of Shiraz plain unconfined aquifer using Aquifer Test software. The Second International Conference on New Research Findings in Science, Engineering and Technology.

Mintenig, S.M., Loder, M.G.J., Primple, S., Gerdts, G., 2019. Low numbers of microplastics detected in drinking water from ground water sources. Science of the Total Environment 648, 631-635.

Ng, E. L., Lwanga, E. H., Eldridge, S. M., Johnston, P., Hu, H. W., Geissen, V., Chen, D., 2018. An overview of microplastic and nanoplastic pollution in agroecosystems. Science of the Total Environment 627, 1377-1388.

O'Connor, D., Pan, S., Shen, Z., Song, Y., Jin, Y., Wu, W.M., Hou, D., 2019. Microplastics undergo accelerated vertical migration in sand soil due to small size and wet-dry cycles. Environmental Pollution 249, 527-534.

Oren, O., Yechieli, Y., Böhlke, J.K., Dody, A., 2004. Contamination of groundwater under cultivated fields in an arid environment, central Arava Valley, Israel. Journal of Hydrology 290, 312-328.

Panno, S.V., Kelly, W.R., Scott, J., Zheng, W., McNeish, R.E., Holm, N., Hoellein, T.J., Baranski, E.L., 2019. Microplastic contamination in karst groundwater systems. Groundwater 57, 189-196.

Rezaeia, M., Abbasi, S., Oleszczuk, P., Pourmahmoodd, H., Ritsema, C., Turner, A., 2022. Microplastics in agricultural soils and their transport by wind erosion. Submitted.

Rodríguez-Estrella, T., 2012. The problems of overexploitation of aquifers in semi-arid areas: the Murcia Region and the Segura Basin (South-east Spain) case. Hydrology and Earth System Science Discussions 9, 5729-5756.

Samandra, S., Johnston, J.M., Jaeger, J.E., Symons, B., Xie, S., Currell, M., Ellis, A.V., Clarke, B.O., 2022. Microplastic contamination of an unconfined groundwater aquifer in Victoria, Australia. Science of the Total Environment 802, 149727.

Samani, N., 2001. Response of karst aquifers to rainfall and evaporation, Maharlu Basin, Iran. Journal of Cave and Karst Studies 63, 33-40.

Scanlon, B.R., Keese, K.E., Flint, A.L., Flint, L.E., Gaye, C.B., Edmunds, W.M., Simmers, I., 2006. Global synthesis of groundwater recharge in semiarid and arid regions Hydrological Processes 20, 3335-3370.

Tanentzap, A.J., Cottingham, S., Fonvielle, J., Riley, I., Walker, L., Woodman, S.G., Kontou, D., Pichler, C.M., Reisner, E., Lebreton, L., 2021. Microplastics and anthropogenic fibre concentrations in lakes reflect surrounding land use. PLoS Biol 19, e3001389. https://doi.org/10.1371/journal.pbio.3001389